

Two Component Model of Dark Energy

Yan Gong and Xuelei Chen

*National Astronomical Observatories, Chinese Academy of Sciences,
20A Datun Rd, Chaoyang District, Beijing 100012, China*

We consider the possibility that the dark energy is made up of two or more independent components, each having a different equation of state. We fit the model with supernova and gamma-ray burst (GRB) data from recent observations, and use the Markov Chain Monte Carlo (MCMC) technique to estimate the allowed parameter regions. We also use various model selection criteria to compare the two component model with the Λ CDM, one component dark energy model with static or variable w (XCDM), and with other multi-component models. We find that the two component models can give reasonably good fit to the current data. For some data sets, and depending somewhat on the model selection criteria, the two component model can give better fit to the data than XCDM with static w and XCDM with variable w parameterized by $w = w_0 + w_a z/(1+z)$.

I. INTRODUCTION

Observations have shown that more than 2/3 of the total cosmic density is made of an unknown “dark energy”, which cause the expansion of the Universe to accelerate [1, 2]. The cosmological constant, with equation of state $w = -1$, is the simplest form of dark energy, and it fits many observations reasonably well. However, from a fundamental physics point of view, it suffers a fine-tuning problem of 122 order of magnitude. Furthermore, it appears to be a great coincidence for its density to be just comparable to the matter density today [3]. Many alternative models of dark energy, e.g. quintessence[4, 5, 6, 7, 8, 9, 10], phantom[11], quintom[12], K-essence[13, 14], Chaplygin gas[15, 16, 17], and so on, have been proposed, but at present none of these is clearly superior than the cosmological constant. Most of these models consists only a single component of dark energy: either it is phenomenologically described by an equation of state parameter $w : p = w\rho$ (w can vary, and many different forms of parameterization have been introduced), or by a dynamical field, although in some cases two scalar fields are introduced.

In the present paper, we consider dark energy models which consist of two independent components with equation of state w_1 and w_2 respectively. This is motivated by the following considerations. (1) If there is indeed unknown physical laws which give rise dark energy, it may well allow more than one form of it to be present. (2) Furthermore, if one describe dark energy by scalar fields, then they do not necessarily have one single equation of state, especially in the case with multiple fields, it is quite plausible that for each field the corresponding equation of states are different. (3) Some observations [18, 19] seem to favor models with $w < -1$ which necessitate negative kinetic terms (phantoms), or with variable equation of state in which w vary across -1 (quintoms), although in more recent observations [20, 21] these trends are weakened. One may wonder if such unusual behavior could be more naturally explained by considering two dark energy components, with different equation of states, and dominate at different redshifts. For example, in Ref. [22]

two scalar fields were invoked to reproduce the phantom behavior.

We model the two independent dark energy components with equation of state parameter w_1, w_2 , which can either be fixed, or variable with redshift. We use the Markov Chain Monte Carlo (MCMC) technique to find the probability distribution of the models in parameter space, which allows us to see how the two component dark energy model fares with observation. The data we used are supernova type Ia (SN Ia) and GRB data, which is currently the most direct and powerful probe of dark energy. In this analysis we have not included other constraints, esp. the cosmic microwave background (CMB), as we do not expect the fixed effective equation of state description used here is really good at very high redshifts.

To compare our model with single component dark matter models and see if there is indeed any evidence for two component of dark energy, we calculate the best fit χ^2 , as well as the AIC, BIC and Bayesian evidence(BE). The models being compared include the Λ CDM, XCDM (phenomenological model of single component dark energy described by an equation of state), and our two component model $X_1 X_2$ CDM1.

We have used several different data sets to perform our fit, e.g. the Gold04 [18] and Gold06 [19] data set, the SNLS [20] data set, and the ESSENCE data set[21]. There are some differences in the result. To avoid repetition, we presented the result of only one data set in detail, this is a combination of supernovae and GRB data. The supernovae data consists 182 high-quality SN Ia samples¹ selected from the Gold06 [19], SNLS [20] and ESSENCE [21] data sets, which includes 30 HST supernovae, 47 SNLS supernovae from Gold06, 60 ESSENCE supernovae, and 45 nearby supernovae from WV07 [23]. Two different light-curve fitters, MLCS2k2 [24, 25], and SALT [26], are used in these data sets. As they are consistent with each other [19, 21], all of the SN Ia data used here are fitted using MLCS2k2 algorithm to avoid

¹ Although the number of sample coincides with that of Gold06, this is in fact a different data set.

normalization [27]. The GRB data provides a good complement to the SN Ia data [28, 29, 30, 31, 32, 33, 34, 35], as the GRB can be observed at much higher redshift, thus providing a better baseline for detecting variation in the dark energy equation of state. The GRB data set is constituted of 27 GRB samples in Ref. [29], which are generated with the $E_{peak} - E_\gamma$ correlation discovered by Ghirlanda et al.(2004) and is one of the tightest correlation for GRB. We have not used all the 69 GRB samples in that paper, because there is larger uncertainty in the other correlations. The method of calculating μ_{GRB} is described in Ref. [29], but we only use the $E_{peak} - E_\gamma$ correlation in the paper. We marginalize H_0 at last as we did for the supernovae case.

The structure of this paper is as follows: in §2 we present the formalism and methods, including a brief summary of the MCMC approach for computing probability distribution of the parameters, and brief summary of model selection criteria. In §3, the results of our fit are shown. In §4, we will compare a few models. Finally, we summarize our results in §5.

II. METHODS

A. Model

We consider a model of two independent components of dark energy, with static equation of state w_1 and w_2 respectively. The expansion rate $H(z)$ is given by

$$H^2(z) = H_0^2 \Omega(\mathbf{z}; \theta), \quad (1)$$

where, in the flat case:

$$\begin{aligned} \Omega(\mathbf{z}; \theta) = & \Omega_{m_0}(1+z)^3 + \Omega_{x_1}(1+z)^{3(1+w_1)} \\ & + (1 - \Omega_{m_0} - \Omega_{x_1})(1+z)^{3(1+w_2)} \end{aligned} \quad (2)$$

and in the non-flat case:

$$\begin{aligned} \Omega(\mathbf{z}; \theta) = & (1 - \Omega_{m_0} - \Omega_{x_1} - \Omega_{x_2})(1+z)^2 + \Omega_{m_0}(1+z)^3 \\ & + \Omega_{x_1}(1+z)^{3(1+w_1)} + \Omega_{x_2}(1+z)^{3(1+w_2)} \end{aligned} \quad (3)$$

Here θ is the cosmological parameter set consisting of

$$\theta = \begin{cases} (\Omega_{m_0}, \Omega_{x_1}, w_1, w_2) & \text{in flat case} \\ (\Omega_{m_0}, \Omega_{x_1}, \Omega_{x_2}, w_1, w_2) & \text{in non-flat case} \end{cases} \quad (4)$$

The luminosity distance can be written as

$$d_L(z; \theta) = (1+z)|\Omega_k|^{-\frac{1}{2}} \text{sinn} \left\{ |\Omega_k|^{\frac{1}{2}} \times \int_0^z \frac{cdz'}{H(z')} \right\}, \quad (5)$$

where $\text{sinn}(x) = \sinh(x)$, x , $\sin(x)$ for open, flat and close geometries respectively.

B. Analysis

Given a cosmological model defined by n parameters $\theta = (\theta_1, \dots, \theta_n)$, and a data set consist of N quantities

$\mathbf{d} = (d_1, \dots, d_N)$ with Gaussian-distributed errors $\sigma_{\mathbf{d}} = (\sigma_1, \dots, \sigma_N)$, the likelihood function can be written as:

$$\mathcal{L}(\mathbf{d}|\theta) = \frac{1}{\sqrt{2\pi}\sigma_{\mathbf{d}}} e^{-\frac{1}{2}\chi^2}, \quad (6)$$

where for un-correlated data points,

$$\chi^2(\theta) = \sum_{i=1}^N \frac{(d_i^{obs} - d_i^{th})^2}{\sigma_i^2}. \quad (7)$$

If both SN Ia data and GRB data are used, we have

$$\chi^2 = \chi_{SN_{sel}}^2 + \chi_{GRB}^2. \quad (8)$$

For the SN Ia data,

$$\chi_{SN}^2(\theta) = \sum_{i=1}^N \frac{(\mu_{obs}(z_i) - \mu_{th}(z_i))^2}{\sigma_i^2}, \quad (9)$$

where the theoretical value of distance modulus $\mu_{th}(z_i)$ is given by

$$\begin{aligned} \mu_{th}(z_i) = & 5 \log_{10} d_L(z_i) + 25 \\ = & 5 \log_{10} D_L(z_i) - 5 \log_{10} h_0 + 42.38, \end{aligned} \quad (10)$$

and

$$D_L(z) = \frac{H_0}{c} \times d_L(z). \quad (11)$$

The Hubble constant $H_0 = 100h_0 \text{kms}^{-1} \text{Mpc}^{-1}$ may be marginalized over as a nuisance parameters, as described in [36], and we would obtain

$$\chi_{SN_{sel}}^2(\theta) = A(\theta) - \frac{B^2(\theta)}{C}, \quad (12)$$

where

$$\begin{aligned} A(\theta) = & \sum_{i=1}^N \frac{(\mu_{obs}(z_i) - 5 \log_{10}(D_L(z_i)))^2}{\sigma_i^2} \\ B(\theta) = & \sum_{i=1}^N \frac{\mu_{obs}(z_i) - 5 \log_{10}(D_L(z_i))}{\sigma_i^2} \\ C = & \sum_{i=1}^N \frac{1}{\sigma_i^2} \end{aligned} \quad (13)$$

Alternatively, we can integrate over H_0 , and be left with an additional constant term $\ln(C/2\pi)$ which would not affect our results given a data set[36, 37, 38].

C. MCMC

Given an observational data set \mathbf{d} , the posterior distribution of a parameter set θ is, according to the Bayes theorem,

$$\mathbf{p}(\theta|\mathbf{d}) = \frac{\mathcal{L}(\mathbf{d}|\theta) \mathbf{p}(\theta)}{\int \mathcal{L}(\mathbf{d}|\theta) \mathbf{p}(\theta) \mathbf{d}\theta}, \quad (14)$$

where $\mathbf{p}(\theta)$ is the prior probability distribution, and $\mathcal{L}(\mathbf{d}|\theta)$ is the likelihood for obtaining the data set \mathbf{d} given the parameter set θ and is given by Eq. 6. To obtain the posterior probability distribution of the parameters, we employ the MCMC technique to generate random samples in the parameter space. This method has several advantages over grid-based approach. Most importantly, the computational time cost increases linearly with the number of parameters, so even for a large number of parameters the estimate can be done within an acceptable computation time. Additionally, since the MCMC method generate samples from the full posterior distribution, it gives far more information than the marginalized distributions[39, 40, 41], and dose not require a Gaussian distribution of the likelihood[42].

With the MCMC technique, a chain of sample points which is distributed in the parameter space according to $\mathbf{p}(\theta|\mathbf{d})$ is generated by Monte Carlo. The Metropolis-Hastings algorithm with uniform prior probability distribution is used to decide whether to accept a new point into the chain by an acceptance probability:

$$\begin{aligned} \mathbf{a}(\theta_{n+1}|\theta_n) &= \min \left\{ \frac{\mathbf{p}(\theta_{n+1}|\mathbf{d}) \mathbf{q}(\theta_n|\theta_{n+1})}{\mathbf{p}(\theta_n|\mathbf{d}) \mathbf{q}(\theta_{n+1}|\theta_n)}, \mathbf{1} \right\} \\ &= \min \left\{ \frac{\mathcal{L}(\mathbf{d}|\theta_{n+1}) \mathbf{q}(\theta_n|\theta_{n+1})}{\mathcal{L}(\mathbf{d}|\theta_n) \mathbf{q}(\theta_{n+1}|\theta_n)}, \mathbf{1} \right\} \end{aligned} \quad (15)$$

where $\mathbf{q}(\theta_{n+1}|\theta_n)$ is the proposal density of proposing a new point θ_{n+1} given a current point θ_n in the chain. If $\mathbf{a} = 1$, the new point θ_{n+1} is accepted; otherwise, the new point is accepted with probability \mathbf{a} . The trials are repeated until a new point is accepted, and then we set $\theta_n = \theta_{n+1}$. In our computation, we set a uniform Gaussian-distributed proposal density for every point which is independent of the position on the chain, so that $\mathbf{q}(\theta_{n+1}|\theta_n)$ and $\mathbf{q}(\theta_n|\theta_{n+1})$ are cancelled, we then have

$$\mathbf{a}(\theta_{n+1}|\theta_n) = \min \left\{ \frac{\mathcal{L}(\mathbf{d}|\theta_{n+1})}{\mathcal{L}(\mathbf{d}|\theta_n)}, \mathbf{1} \right\}. \quad (16)$$

We assume uniform prior for the parameters within the given ranges. We have made tests with various ranges, for the results presented here we have adopted the following: $\Omega_{m_0} \in (0, 1)$, $\Omega_{x_1} \in (0, 2)$, $\Omega_{x_2} \in (0, 2)$, $w_1 \in (-20, 5)$ and $w_2 \in (-20, 5)$. We have considered also the special case of flat geometry case, for which $\Omega_{x_1} \in (0, 1 - \Omega_{m_0})$ is set, so that $\Omega_{x_2} = 1 - \Omega_{m_0} - \Omega_{x_1} \geq 0$, assuming the energy density of all the components are non-negative.

Although the chains will eventually “burn in” even given a random position in the parameter-space, in practice we have chosen initial points near the maximum likelihood point so that computational time is saved[43].

The proposal density have an important effect for good convergence and mixing of a chain, and the step provided by proposal density should not be either too large or small that may lead to slow convergence or mixing [39,

43, 44, 45, 46, 47, 48, 49, 50]. The method we use to determine the proposal density is a adaptive step size Gaussian sampler described in Ref. [46]. We use the criterion proposed by Gelman and Rubin (1992) to test convergence and mixing of the chains, and after that we freeze in the the proposal density [46, 51].

We generate six chains for each case we study, and about seventy thousands points are sampled in each chain. After the burn-in process and thinning the chains, we merge them into one chain which consists of about 10000 points used to generate the probability distribution of the parameters. As the two dark energy components are completely symmetric for Monte Carlo, when plotting the data we have also made “mirrow” points for each point on the chain $((\Omega_1, w_1) \leftrightarrow (\Omega_2, w_2))$.

D. Model selection criteria

We shall compare our two component models with one dark energy component models. As the number of parameters differ, the simple χ^2 statistic is not always effective. We therefore consider several model selection criteria introduced in the literature [52, 53, 54].

The Akaike information criterion (AIC) [55] is defined as

$$\text{AIC} = -2 \ln \mathcal{L}_{max} + 2k, \quad (17)$$

where \mathcal{L}_{max} is the maximum likelihood and k is the number of parameters in the model [53, 56, 57]. The second term penalizes models with more parameters. However, the size of the data set is not considered by the AIC, thus when we have very large number of data points, the reduction on χ^2 due to additional parameters would also be very large, and one may still mis-select the model using the AIC criterion [52].

The Bayesian information criterion [58] can be written as

$$\text{BIC} = -2 \ln \mathcal{L}_{max} + k \ln N, \quad (18)$$

which includes the penalization of the number of data N . Nevertheless, the BIC tends to over penalize the number of parameters, given large number of data and is an approximation of the Bayesian evidence on some assumptions that may not be valid in practice, and it dose not take the full advantage of Bayesian technique [52, 54, 56]

The Bayesian evidence (BE) of a model M takes the form

$$\text{BE} = \int \mathcal{L}(\mathbf{d}|\theta, M) \mathbf{p}(\theta|M) d\theta, \quad (19)$$

which is just the denominator of equation(14). The BE is the average of the likelihood of a model weighted by its prior in the parameter space. It automatically includes the penalties of the number of parameters and data, so it is believed to be more direct, reasonable and unambiguous than the χ^2_{min} and ICs in model selection

[53, 59, 60, 61, 62, 63, 64, 65, 66]. The logarithm of BE can be used as a guide for comparing models (Jeffreys 1961), and we choose the Λ CDM as the referenced model for comparison: $\Delta \ln(\text{BE}) = \ln(\text{BE})_{\text{model}} - \ln(\text{BE})_{\Lambda\text{CDM}}$. The strength of the evidence for the model is considered according to the numerical value of BE:

$$\begin{cases} \Delta \ln \text{BE} < 1 & \text{Weak} \\ 1 < \Delta \ln \text{BE} < 2.5 & \text{Significant} \\ 2.5 < \Delta \ln \text{BE} < 5 & \text{Strong to very strong} \\ \Delta \ln \text{BE} > 5 & \text{Decisive} \end{cases} \quad (20)$$

We use the nested sampling algorithm to compute BE [62, 66], and the error is about 0.10.

III. RESULTS

For two component dark energy models, one can define an effective equation of state,

$$w_{\text{eff}}(z) = \frac{w_1 \Omega_{x1}(z) + w_2 \Omega_{x2}(z)}{\Omega_{x1}(z) + \Omega_{x2}(z)}. \quad (21)$$

In Fig. 1 we show the distance modulus μ and equation of state w_{eff} for a few examples of two component dark energy model, together with the Λ CDM model and an one-component dark energy model for reference. As can be seen from these examples, the phantom divide line ($w = -1$) is easily crossed, which is not unexpected if one component has $w > -1$ and another has $w < -1$. The w_{eff} and μ curves are very smooth, and the two component model can fit the current data pretty well. Indeed, from these curves we may take note of the following character of the two component model $X_1 X_2 \text{CDM1}$: the effective dark energy equation of state approaches that of a constant value at high redshift, then it make transition to another value at some lower redshift. $X\text{CDM2}$, the one component dark energy model with variable equation of state with the usual parametrizations, can not realize this easily. Inspecting the fit to the distance moduli curve, it is not easy to distinguish between these models from each other, or from the Λ CDM model and the one component dark energy model, despite their apparant difference in the $w_{\text{eff}}(z)$. The error on w derived from current data is still too large (the $1 - \sigma$ error on w for the one component model is plotted as yellow dashed lines in Fig. 1).

We now investigate the fit of the two component models more quantitatively, with MCMC simulation. We have performed our fit with several different combinations of data sets. We found that the general features of the results are all very similar. Here we present only one data set of $\text{SN}_{\text{sel}} + \text{GRB}$ in detail. We plot the PDF of Ω_{m0} in Fig. 2. The PDF of Ω_{m0} peaks at 0.37 (0.22) for flat (generic) geometry. This value is typical for SN Ia only fit, but greater than those based on the combined fit to SN Ia, CMB and LSS data. As we have mentioned in the introduction, the purpose of this paper is to study the effect of two component dark energy on low redshift SN

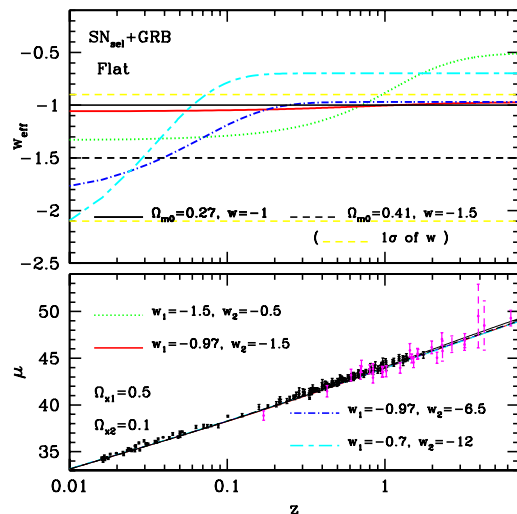


FIG. 1: The w_{eff} (upper panel) and luminosity distance modulus μ (lower panel) for four two component models, marked with red(solid), green (dot), blue (short dash dot) and cyan (long dash dot) lines. All these models have flat geometry and $\Omega_{x1} = 0.5, \Omega_{x2} = 0.1$, but with different w_1, w_2 . These model gave good (but not the best) fit to the data amongst the two component models. For comparison, the Λ CDM model with $\Omega_{m0} = 0.27$ and the one component model with $\Omega_{m0} = 0.41, w = -1.5$ are plotted. For the latter, we also plot the $1 - \sigma$ error on w in yellow (dashed) line. In the μ plot, we show the SN and GRB data points and error bars in black and pink respectively.

Ia fits, we do not include CMB data. There is some difference in the best fit (maximal point of the PDF curve) value of Ω_{m0} in the one and two component models, but the difference is not too large.

The PDF of one of the dark energy component, Ω_{x1} is plotted in Fig. 3. For reference, we have also plotted the PDF of dark energy density in one-component dark energy models. Let us consider the flat case first. The PDF has a high plateau at $\Omega_{x1} < 0.65$ but declines sharply above that. As we have $\Omega_{m0} + \Omega_{x1} < 1$ and $\Omega_{m0} > 0$, this result is not surprising. There are also relatively small peaks and two small troughs on the high plateau: the peaks at 0.16 and 0.54, and troughs at 0.02 and 0.37. We shall study the nature of these in the following paragraphs. However, the peaks and troughs are not too large: the amplitude is about 1/10 of the average. For the non-flat model, there is a single peak at 0.2, and the PDF declines above the peak, but has a small low plateau between 0.45 to 0.65.

In Fig. 4 we plot the histogram for the distribution of the equation of state parameter w_1 . Again, for reference purpose we also plotted the distribution for one component dark energy models. For both the flat and general geometry case, the peak of the distribution is near $w = -1$. However, for all these distributions there are a long tails at $w_1 \ll -1$, for the non-flat case the tail is more extended.

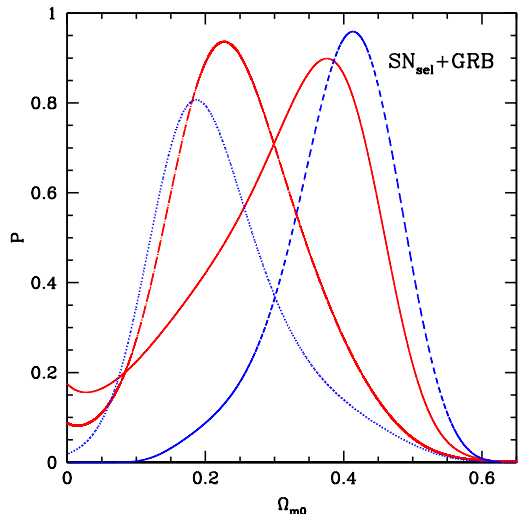


FIG. 2: The one dimensional PDF of Ω_{m0} . The red solid line is for case of flat geometry, the red dot-dashed line for generic geometry. As a comparison, the PDF of one component model with static w are shown, and the blue dashed line is for flat geometry, the blue dotted line for generic geometry.

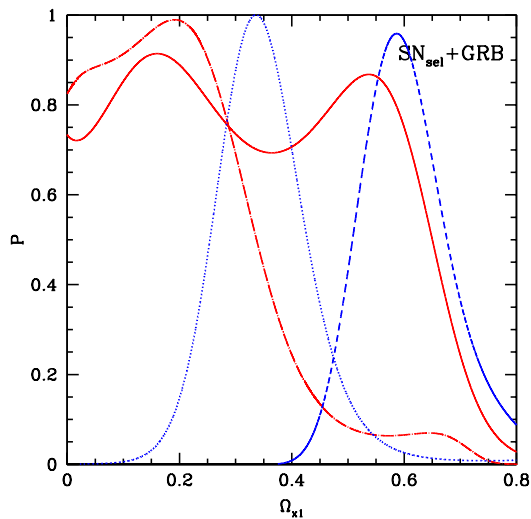


FIG. 3: The one dimensional PDF of Ω_{x1} . Red solid line: flat; red dot-dashed line: generic. For one component model with static w , blue dashed line: flat; blue dotted line: generic.

In Fig. 5 we plot the distribution of Ω_{x1} vs. w_1 . We can see that the density peak of the distribution is at $\Omega_{x1} \sim 0.55, w_1 \sim -1$. This corresponds well with the peak in the PDF of Ω_{x1} and w_1 . On the other hand, we note that the distribution also spans to much negative value of w_1 with small Ω_{x1} : the addition of a small fraction of very negative equation of state component (phantom) is allowed by the data. On the other hand, for these deep phantom, large Ω_{x1} is not allowed, leaving a conspicuous blank lower right half. The distribution do extends to a “pier” at $w_1 = -1, \Omega_{x1} > 0.6$. These are similar to

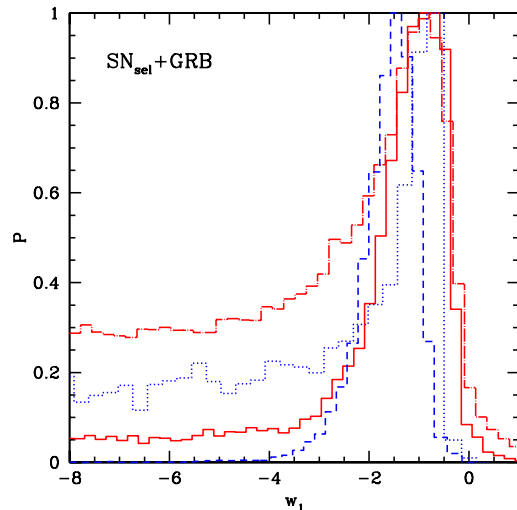


FIG. 4: The PDF of equation of state parameter w_1 , and one component model are also shown.

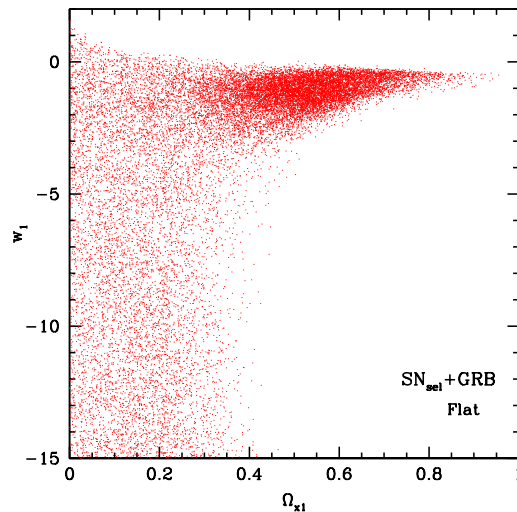


FIG. 5: The point distribution of $\Omega_{x1}-w_1$.

Λ CDM in the parameter space. There is also some points on the corner with $w_1 > 0$.

In the above we have looked at the distribution of one component in our two components model. Now we can also examine how the two components are related. The scatter plot of $\Omega_{x1}\Omega_{x2}$ is shown in Fig. 6. Since $\Omega_{x1} + \Omega_{x2} = 1 - \Omega_{m0}$, it is very nature to see that there is a linear anti-correlation between Ω_{x1} and Ω_{x2} . Apparently, the region with $0.4 < \Omega_{x1} + \Omega_{x2} < 0.7$ has greater density of points, furthermore, in this region, there is a decrease of point density near $\Omega_{x1} = \Omega_{x2}$.

We show the scatter plot and associated contours for $w_1 w_2$ in Fig. 7. Near the $w_1 = w_2$ diagonal the PDF is highest. Models in this region is very similar to one component dark energy. As we already know, the one

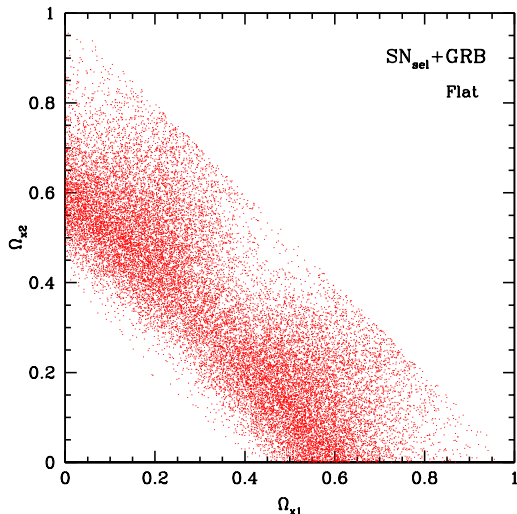


FIG. 6: The point distribution of energy density for the two components.

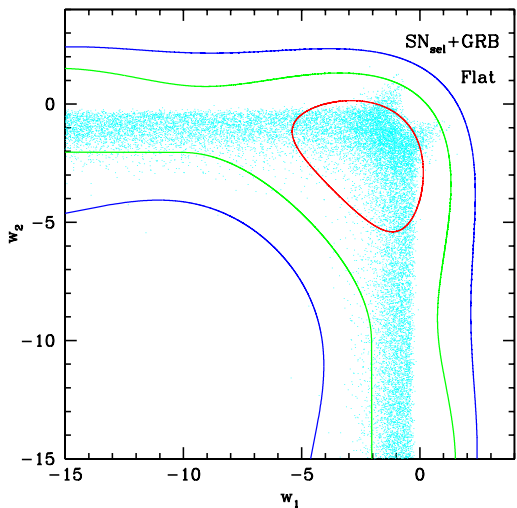


FIG. 7: The point distribution and contour map of equation of state for the two components. The 1σ (68.3%), 2σ (95.5%) and 3σ (99.7%) confidence levels are marked by red, green and blue solid lines respectively.

component dark energy model fits reasonably well the SN Ia data, so this result is not surprising. However, we note that points far from the diagonal are also allowed, indeed the allowed region is extends to very large negative w . These models have one dark energy component which has $-2 < w < 0$, and another component whose w can be smaller or much smaller than -1.

Another way to see how the two components are related is to plot their differences, as shown in Fig. 8, for $|\Omega_{x1} - \Omega_{x2}|$ vs $|w_1 - w_2|$. First, we note that the points expands to very high value of $|w_1 - w_2|$, showing that the two components can be very different. Secondly,

these high difference points are widely distributed from $|\Omega_{x1} - \Omega_{x2}| = 0$ to 0.5. This tells us that it is not the case that one single component always dominates. Nevertheless, we can see that at $|\Omega_{x1} - \Omega_{x2}| \sim 0.4$ the points are indeed somewhat more frequent.

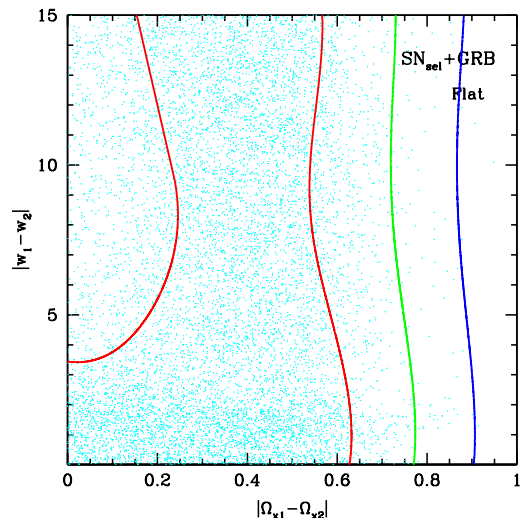


FIG. 8: The difference of the two components.

IV. MODEL COMPARISONS

In this section we compare the two component model considered in this paper with several different models. We calculate their χ^2_{min} , as well as several frequently used model selection criteria, namely AIC, BIC and BE. The following models are considered: Λ CDM, XCDM1, XCDM2, X_1X_2 CDM1, X_1X_2 CDM2, $X_1X_2X_3$ CDM (see Table 1). XCDM1 is an one component dark energy model with static w ; XCDM2 is an one component model with variable w parameterized by $w = w_0 + w_a z / (1 + z)$; X_1X_2 CDM1 is the two component model discussed extensively in this paper. We also calculate the statistics of other two kind of multi-component models: X_1X_2 CDM2 is two components model with variable w parameterized by $w_1 + w_{1a}z / (1 + z)$ and $w_2 + w_{2a}z / (1 + z)$; $X_1X_2X_3$ CDM is a three component model with static w .

With different data set, the best fit result is also different. Here we consider several different data sets: (1) the selected supernovae samples and GRB samples, for which detailed result is presented in the last section; (2) the selected supernovae sample, but without GRB; (3) 182 supernovae known as the Gold06 sample (4) The SNLS sample, which includes 115 supernovae sample published in Ref. [20], for this sample the parameters α and β are joined into our cosmological parameter set to estimate the statistics; (5) the ESSENCE data set, which consists of two parts: 60 ESSENCE samples and 45 nearby SN Ia published in Ref. [21].

Using the above data sets, we calculate the χ^2 and other model selection criteria. Our calculation is done for flat and non-flat geometric prior separately. The results are given in Table 2 and Table 3.

First we look at the flat case. It is clear that with additional parameters, the χ^2 can always be reduced for models with more parameters, hence it not very useful in comparing models with different number of parameters[67]. On the other hand, using different model selection criteria, the conclusion we draw could differ. The BIC strongly penalizes models with more parameters, so models with less parameters almost always win. For the AIC, the results varies with different data set. For the selected SNIa data set SN_{sel} (which are selected for the best data) and $\text{SN}_{\text{sel}} + \text{GRB}$ data set, the $X_1X_2\text{CDM1}$ fares as well as $X\text{CDM1}$ (the one component dark energy model with fixed w), and better than the $X\text{CDM2}$ (the one component dark energy model with variable w). In the ESSENCE data set, the $X_1X_2\text{CDM1}$ fits almost as well as $X\text{CDM1}$ and better than $X\text{CDM2}$. In the Gold 06 and SNLS data sets, however, the one component models fit better than two component models.

Perhaps the most accurate model selection criterion considered here is BE. Comparing to ΛCDM , for most data set the two component model $X_1X_2\text{CDM1}$ is slightly disfavored using BE (except for the ESSENCE data set, for which it is slightly favored). However, the evidence of this disfavorance is weak. In comparison, the one component dark energy model $X\text{CDM1}$ and $X\text{CDM2}$ are significantly disfavored when compared with the ΛCDM . We also found that $X_1X_2\text{CDM2}$ and $X_1X_2X_3\text{CDM}$ have comparable BE.

While we have reason from both theory (inflation) and observation (CMB) to suppose that the geometry of observable universe is flat, for generality we also consider non-flat geometry. In the non-flat case, again with different data sets the result are somewhat different. Generally, however, the data seems to be less favorable for two component dark energy models. For example, with $\text{SN}_{\text{sel}} + \text{GRB}$ data set, the $X_1X_2\text{CDM1}$ is significantly disfavored over ΛCDM , which is similar to $X\text{CDM1}$, while the $X\text{CDM2}$ is only slightly disfavored. However, $X_1X_2\text{CDM2}$ and $X_1X_2X_3\text{CDM}$ is slightly favored. We suppose that in the non-flat model, the curvature term behavior is degenerate with a special form of dark energy component, which makes the model less favored by the model selection criteria.

V. CONCLUSION

In this paper we considered phenomenological multi-component dark energy models, in particular a two component model with static equation of state w_1 and w_2 , and examined how good can they fit the supernovae and GRB data. We have tested our models with several recently published data sets. For most of the analysis, we have used a high quality data set with 182 SN Ia sample

and 27 GRB sample selected from resent observations. The MCMC technique is used in our cosmological parameter fitting, and to compare different models we have tried several frequently used model selection criteria.

The fitting results indicate that the two component models can fit the current data set fairly well. The effective equation of state of the dark energy can cross the phantom divide line, as would have been expect for a model with one component $w > -1$ and another $w < -1$.

We have compared the multi-component models with the ΛCDM model and one component models using several model selection criteria, including χ^2 , AIC, BIC, and BE. The result varies for different choice of model selection criteria and data set. The BIC almost always favor models with less parameters. For AIC, we found different results for different data sets. Since the Bayesian evidence (BE) is presently considered to be better than either AIC or BIC, we have mainly focused on the results derived using BE. Using BE, we found that for flat geometry the multi-component models can fit as well as the ΛCDM model, and for all of the data sets, which is worthy of note, the multi-component models fit significantly ($\Delta \ln(\text{BE}) \gtrsim 1$) better than one component models.

The model selection technique has been applied to dark energy model studies in several recent works. For the most recent data, the ΛCDM model is favored over models with simply parametrized variable equation of state models such as $X\text{CDM1}$ and $X\text{CDM2}$ [68, 69]. We have reached the same conclusion for these models. Because the data set and constraining technique used in each case is different (e.g., in Ref. [68], SNIa Gold 06 data set, together with CMB shift parameter and SDSS BAO result is used), it is difficult to make a full comparison. We note, however, that for $X\text{CDM1}$ and $X\text{CDM2}$ they obtained $\Delta \ln(\text{BE}) = -1.027, -1.118$ (with respect to ΛCDM) respectively. We have not used the CMB and BAO data in our calculation, but for the Gold 06 data set, we found $\Delta \ln(\text{BE}) = -1.60, -1.16$ respectively, which are of similar strength.

It is premature to say at this stage whether single or multiple component dark energy model is favored, as the evidence is still weak. Even if in the future we find that multi-component model is preferred in a fit, we note that this is only a phenomenological model based on parametrization. It is conceivable that dark energy of a single physical origin could give rise to the appearance of multiple components with different equation of state. Nevertheless, our investigation show that multiple component is allowed by current data. When one discusses the properties of dark energy as inferred from observations, this possibility should not be neglected.

Acknowledgments

Our MCMC chain computation was performed on the Supercomputing Center of the Chinese Academy of Sciences and the Shanghai Supercomputing Center. This

work is supported by the National Science Foundation of China under the Distinguished Young Scholar Grant 10525314, the Key Project Grant 10533010, by the Chinese Academy of Sciences under grant KJCX3-SYW-N2,

and by the Ministry of Science and Technology under the national basic sciences program (973) under grant 2007CB815401.

-
- [1] S. Perlmutter et al., *Astrophys. J.* **517**, 565 (1999)
- [2] A. G. Riess et al., *Astron. J.* **116**, 1009 (1998)
- [3] For a review, see e.g. S. M. Carroll, *Living Rev. Relativity.* **4**, 1 (2001) (astro-ph/0004075).
- [4] C. Wetterich, *Nucl. Phys. B* **302**, 668 (1988)
- [5] B. Ratra and Peebles, *Phys. Rev. D* **37**, 321 (1988)
- [6] P. G. Ferreira and M. Joyce, *Phys. Rev. Lett.* **79**, 4740 (1997); *Phys. Rev. D* **58**, 023503 (1998).
- [7] R. R. Caldwell, R. Dave, P. J. Steinhardt, *Phys. Rev. Lett.* **80**, 1582 (1998).
- [8] E. J. Copeland, A. R. Liddle, D. Wands, *Phys. Rev. D* **57**, 4686 (1998).
- [9] S. M. Carroll, *Phys. Rev. Lett.* **81**, 3067 (1998).
- [10] I. Zlatev, L. M. Wang, P. J. Steinhardt, *Phys. Rev. Lett.* **82**, 896 (1999); P. J. Steinhardt, L. M. Wang, I. Zlatev, *Phys. Rev. D* **59**, 123504 (1999).
- [11] R. R. Caldwell, *Phys. Lett. B* **545**, 23 (2002)
- [12] B. Feng, X. Wang, X. Zhang, *Phys. Lett. B* **607**, 35 (2005).
- [13] T. Chiba, T. Okabe and M. Yamaguchi, *Phys. Rev. D* **62**, 023511 (2000)
- [14] C. Armendariz-Picon, V. Mukhanov and P. J. Steinhardt, *Phys. Rev. Lett.* **85**, 4438 (2000); *Phys. Rev. D* **63**, 103510 (2001).
- [15] A. Y. Kamenshchik, U. Moschella and V. Pasquier, *Phys. Lett. B* **511**, 265 (2001)
- [16] N. Bilic, G. B. Tupper and R. D. Viollier, *Phys. Lett. B* **535**, 17 (2002)
- [17] M. C. Bento, O. Bertolami and A. A. Sen, *Phys. Rev. D* **66**, 043507 (2002)
- [18] A. G. Riess et al., *Astrophys. J.* **607**, 665 (2004)
- [19] A. G. Riess et al., *Astrophys. J.* **656**, (2007)
- [20] P. Astier et al., *Astron. Astrophys.* **447**, (2006)
- [21] W. M. Wood-Vasey et al., (2007) astro-ph/0701041
- [22] E. Elizalde, S. Nojiri, S. D. Odintsov, *Phys. Rev. D* **70**, 043539 (2004); see also Shin'ichi Nojiri and S. D. Odintsov, *Gen.Rel.Grav.* **38**, 1285-1304 (2006); S. Capozziello, S. Nojiri and S. D. Odintsov, *Phys. Lett. B* **632**, 597-604 (2006)
- [23] S. Nesseris and L. Perivolaropoulos, *JCAP.* **0702**, 025 (2007)
- [24] A. G. Riess, W. H. Press and R. P. Kirshner, *Astrophys. J.* **473**, 88 (1996)
- [25] S. Jha, A. G. Riess, R. P. Kirshner, *Astrophys. J.* **659**, 122-148 (2007)
- [26] J. Guy, P. Astier, S. Nobili, N. Regnault and R. Pain, *A&A* (2005)
- [27] T. M. Davis et al. (2007) astro-ph/0701510
- [28] G. Ghirlanda et al., *Astrophys. J. Lett.* **613**, L13 (2004)
- [29] B. E. Scafer, *Astrophys. J.* **660**, 16 (2007)
- [30] E. Liang and B. Zhang, *Astrophys. J.* **633**, 611-623 (2005)
- [31] G. Ghirlanda, G. Ghisellini and C. Firmani, *New J.Phys.* **8**, 123 (2006)
- [32] Z. G. Dai, E. W. Liang and D. Xu, *Astrophys.J.* **612** L101-L104 (2004)
- [33] D. Xu, Z. G. Dai and E. W. Liang, *Astrophys. J.* **633**, 603-610 (2005)
- [34] C. Firmani, G. Ghisellini, G. Ghirlanda and V. Avila-Reese, *Mon. Not. R. Astron. Soc.* **360**, LL1 (2005)
- [35] D. Hooper and S. Dodelson, *Astropart. Phys.* **27**, 113-118 (2007)
- [36] S. Nesseris and L. Perivolaropoulos, *Phys. Rev. D* **72**, 123519 (2005)
- [37] S. Nesseris and L. Perivolaropoulos, *Phys. Rev. D* **70**, 043531 (2004)
- [38] M. Goliath et al. (2001) astro-ph/0104009
- [39] A. Lewis and S. Bridle, *Phys. Rev. D* **66**, 103511 (2002)
- [40] D. J. C. MacKay, *Information Theory, Inference, and Learning Algorithms* (2003)
- [41] R. M. Neal, *Probabilistic Inference Using Markov Chain Monte Carlo Methods* (1993)
- [42] L. Perotto et al., *JCAP.* **0610**, 013 (2006)
- [43] H. K. Eriksen et al., *Astrophys.J.* **641**, (2006)
- [44] CosmoMC: <http://cosmologist.info/cosmomc>.
- [45] N. Christensen and R. Meyer, (2000) astro-ph/0006401
- [46] M. Doran and C. M Muller, (2004) astro-ph/0311311
- [47] M. Tegmark et al., *Phys. Rev. D* **69**, 103501 (2004)
- [48] A. Hajian, (2006) astro-ph/0608679
- [49] K. M. Hanson, *SPIE.* **4322**, pp. 456-467 (2001)
- [50] L. Verde et al., *Astrophys. J. Suppl.* **148**, 195 (2003)
- [51] CMBeasy: <http://www.cmbeasy.org>.
- [52] A. R. Liddle, *Mon. Not. R. Astron. Soc.* **351**, L49-53 (2004)
- [53] A. R. Liddle, P. Mukherjee, D. Parkinson, *A&G* **47** 4.30-4.33 (2006)
- [54] A. Kurek and M. Szydlowski, astro-ph/0702484;
- [55] H. Akaike, *IEEE Trans. Auto. Control* **19**, 716 (1974).
- [56] M. Biesiada, *JCAP.* **0702**, 003 (2007)
- [57] W. Godlowski and M. Szydlowski, *Phys. Lett. B* **623**, 10 (2005); M. Szydlowski and W. Godlowski, *Phys. Lett. B* **639**, 5 (2006);
- [58] G. Schwarz, *Annals of Statistics* **6**, 461-464 (1978)
- [59] A. R. Liddle, (2006) astro-ph/0701113
- [60] M. V. John and J. V. Narlikar, *Phys. Rev. D* **65**, 043506 (2002)
- [61] R. Trotta, *Mon. Not. R. Astron. Soc.* **378**, 72-82 (2007)
- [62] P. Mukherjee, D. Parkinson and A. R. Liddle, *Astrophys.J.* **638** L51-L54 (2006)
- [63] P. Mukherjee, D. Parkinson, P. S. Corasaniti, A. R. Liddle and M. Kunz, *MNRAS*, **369** (2006)
- [64] M. Kunz, R. Trotta and D. R. Parkinson, *Phys. Rev. D* **74**, 023503 (2006)
- [65] R. Trotta (2007) astro-ph/0703063
- [66] J. Skilling, <http://www.inference.phy.cam.ac.uk/bayesys/>
- [67] For discussion on this point, see E. V. Linder and R. Miquel, astro-ph/0702542; and A. R. Liddle et al, astro-ph/0703285.
- [68] P. Serra, A. Heavens and A. Melchiorri, *Mon. Not. R. Astron. Soc.* **379**, 1,169 (2007)

TABLE I: $H(z)$ of the models

Model	Flat	Non-flat
Λ CDM	$H^2(z) = H_0^2[\Omega_{m0}(1+z)^3 + (1-\Omega_{m0})]$	$H^2(z) = H_0^2[\Omega_{m0}(1+z)^3 + \Omega_{\Lambda0} + (1-\Omega_{m0}-\Omega_{\Lambda0})(1+z)^2]$
XCDM1	$H^2(z) = H_0^2[\Omega_{m0}(1+z)^3 + (1-\Omega_{m0})(1+z)^{3(1+w)}]$	$H^2(z) = H_0^2[\Omega_{m0}(1+z)^3 + \Omega_x(1+z)^{3(1+w)} + (1-\Omega_{m0}-\Omega_x)(1+z)^2]$
XCDM2	$H^2(z) = H_0^2[\Omega_{m0}(1+z)^3 + (1-\Omega_{m0})(1+z)^{3(1+w+w_a)} e^{3w_a[1/(1+z)-1]}]$	$H^2(z) = H_0^2[\Omega_{m0}(1+z)^3 + \Omega_x(1+z)^{3(1+w+w_a)} e^{3w_a[1/(1+z)-1]} + (1-\Omega_{m0}-\Omega_x)(1+z)^2]$
X ₁ X ₂ CDM1	$H^2(z) = H_0^2[\Omega_{m0}(1+z)^3 + \Omega_{x1}(1+z)^{3(1+w_1)} + (1-\Omega_{m0}-\Omega_{x1})(1+z)^{3(1+w_2)}]$	$H^2(z) = H_0^2[\Omega_{m0}(1+z)^3 + \Omega_{x1}(1+z)^{3(1+w_1)} + \Omega_{x2}(1+z)^{3(1+w_2)} + (1-\Omega_{m0}-\Omega_{x1}-\Omega_{x2})(1+z)^2]$
X ₁ X ₂ CDM2	$H^2(z) = H_0^2[\Omega_{m0}(1+z)^3 + \Omega_{x1}(1+z)^{3(1+w_1+w_{1a})} e^{3w_{1a}[1/(1+z)-1]} + (1-\Omega_{m0}-\Omega_{x1})(1+z)^{3(1+w_2+w_{2a})} e^{3w_{2a}[1/(1+z)-1]}]$	$H^2(z) = H_0^2[\Omega_{m0}(1+z)^3 + \Omega_{x1}(1+z)^{3(1+w_1+w_{1a})} e^{3w_{1a}[1/(1+z)-1]} + \Omega_{x2}(1+z)^{3(1+w_2+w_{2a})} e^{3w_{2a}[1/(1+z)-1]} + (1-\Omega_{m0}-\Omega_{x1}-\Omega_{x2})(1+z)^2]$
X ₁ X ₂ X ₃ CDM	$H^2(z) = H_0^2[\Omega_{m0}(1+z)^3 + \Omega_{x1}(1+z)^{3(1+w_1)} + \Omega_{x2}(1+z)^{3(1+w_2)} + (1-\Omega_{m0}-\Omega_{x1}-\Omega_{x2})(1+z)^{3(1+w_3)}]$	$H^2(z) = H_0^2[\Omega_{m0}(1+z)^3 + \Omega_{x1}(1+z)^{3(1+w_1)} + \Omega_{x2}(1+z)^{3(1+w_2)} + \Omega_{x3}(1+z)^{3(1+w_3)} + (1-\Omega_{m0}-\Omega_{x1}-\Omega_{x2}-\Omega_{x3})(1+z)^2]$

TABLE II: Flat case

Data	Type	Λ CDM	XCDM1	XCDM2	X ₁ X ₂ CDM1	X ₁ X ₂ CDM2	X ₁ X ₂ X ₃ CDM
Gold06 (182)	χ_{min}^2	158.749	156.584	156.405	156.453	155.052	156.430
	AIC	160.749	160.584	162.405	164.453	167.052	168.430
	BIC	163.953	166.992	172.017	177.269	186.404	187.654
	$\Delta \ln(\text{BE})$	-	-1.60	-1.16	-0.68	+0.04	+0.15
SNLS (115)	χ_{min}^2	110.033	110.998	111.008	110.704	110.110	109.707
	AIC	117.033	118.998	121.008	122.704	126.110	125.707
	BIC	125.268	129.978	134.733	139.173	148.070	147.666
	$\Delta \ln(\text{BE})$	-	-1.26	-1.34	-0.36	+0.66	+0.64
ESSENCE (105)	χ_{min}^2	104.531	103.459	103.391	99.469	98.150	97.311
	AIC	106.531	107.459	109.391	107.469	110.150	109.311
	BIC	109.185	112.767	117.388	118.085	126.074	125.235
	$\Delta \ln(\text{BE})$	-	-1.11	-0.91	+0.54	+0.98	+0.94
SN _{sel} (182)	χ_{min}^2	162.508	161.267	161.196	157.332	153.754	155.512
	AIC	164.508	165.267	167.196	165.332	165.754	167.512
	BIC	167.713	171.675	176.808	178.148	184.978	186.737
	$\Delta \ln(\text{BE})$	-	-2.23	-2.70	-0.50	+0.52	+0.40
SN _{sel} + GRB (209)	χ_{min}^2	181.341	180.029	179.988	176.405	174.618	173.466
	AIC	183.341	184.029	185.988	184.405	186.618	185.466
	BIC	186.683	190.713	196.015	197.774	206.672	205.520
	$\Delta \ln(\text{BE})$	-	-2.35	-2.58	-0.31	+0.48	+0.17

[69] R. Lazkoz and E. Majerotto, JCAP. **0707**, 015 (2007)

TABLE III: Non-flat case

Data	Type	ΛCDM	XCDM1	XCDM2	X₁X₂CDM1	X₁X₂CDM2	X₁X₂X₃CDM
Gold06 (182)	χ^2_{min}	156.448	156.447	156.206	156.354	155.303	156.434
	AIC	160.448	162.447	164.206	166.354	169.303	170.434
	BIC	166.856	172.059	177.022	182.374	191.731	192.863
	$\Delta \ln(\text{BE})$	-	-1.45	-1.15	-1.66	-1.07	-1.61
SNLS (115)	χ^2_{min}	111.006	111.066	110.495	110.641	109.711	109.544
	AIC	119.006	121.066	122.495	124.641	127.711	127.544
	BIC	129.986	134.790	138.965	143.855	152.416	152.248
	$\Delta \ln(\text{BE})$	-	-0.80	-0.07	-0.78	+0.46	-0.14
ESSENCE (105)	χ^2_{min}	103.591	99.443	99.393	98.464	98.369	97.303
	AIC	107.591	105.443	107.393	108.464	112.369	111.303
	BIC	112.899	113.405	118.008	121.734	130.947	129.881
	$\Delta \ln(\text{BE})$	-	-1.10	+0.29	-1.07	-0.14	-1.30
SN _{sel} (182)	χ^2_{min}	161.225	158.686	153.607	157.693	153.932	155.108
	AIC	165.225	164.686	161.607	167.693	167.932	169.108
	BIC	171.633	174.298	174.423	183.713	185.156	191.536
	$\Delta \ln(\text{BE})$	-	-1.10	+0.90	-1.34	-0.24	-0.40
SN _{sel} + GRB (209)	χ^2_{min}	180.397	178.631	178.605	176.608	174.446	173.463
	AIC	184.397	184.631	186.605	186.608	188.446	187.463
	BIC	191.082	194.658	199.975	203.319	211.843	210.859
	$\Delta \ln(\text{BE})$	-	-1.32	-0.11	-1.27	+0.08	+0.03